Journal of Thermal Analysis and Calorimetry
https://doi.org/10.1007/s10973-023-12580-9

Effects of thermal cycling on the thermal and magnetic response of Ni–Mn–Sn–Pd alloys

A. Wederni[1] · M. Ipatov[2] · M. Khitouni[3] · J. J. Suñol[1]

Received: 27 February 2023 / Accepted: 17 September 2023

Abstract

Magnetic refrigeration is an option to replace conventional refrigeration. There are many studies that analyze materials with magnetocaloric effect during the first cooling-heating cycle, without analyzing the influence of cycling (necessary to check its applicability). In this work, we proceed to analyze the crystallographic structure (X-Ray diffraction) and the thermal (differential scanning calorimetry) and thermomagnetic (PPMS cycles and ZFC–FH–FC scans) response after a hundred thermal cycles of two Heusler alloys, $Ni_{49}Mn_{36}Sn_{14}Pd_1$ and $Ni_{48}Mn_{36}Sn_{14}Pd_2$ (at.%), that have been produced by melt spinning as ribbon flakes. In order to check its stability from cycling, these ferromagnetic alloys have been subjected to a hundred of thermal cycles (heating/cooling to provoke the austenite to martensite reversible transformation. The comparison before and after cycling behavior allow us to state that the reduction of the crystallographic defects favors higher atomic order. Likewise, the thermodynamic parameters (entropy and enthalpy) and the magnetic response have been reduced at about 10–12%.

Keywords Thermal cycling · Thermal analysis · Heusler · Structural analysis · Thermomagnetic analysis

Introduction

Conventional shape memory is given by applying pressure and/or temperature. In the case of magnetic alloys with shape memory (MSM), this phenomenology occurs not only under pressure and temperature changes, but also when an external magnetic field is applied to the specimens. MSM alloys have their potential applicability as energy transducers, actuators, sensors or in magnetic cooling devices [1]. The application of these materials in magnetic refrigeration needs the study after cycling. The magnetic transition (commonly from ferromagnetism to paramagnetism) must be present. Among the families of alloys with magnetic shape memory are the Heusler alloys [2, 3]. These are characterized by being able to have, in addition to the magnetic transition, the martensitic structural transformation. Between the caloric effects that they can present are magnetocaloric [4], elastocaloric [5] or barocaloric [6]. The martensitic transformation is reversible and presents thermal hysteresis. The Heusler structure, $L2_1$, is a complex cubic structure with an X_2YZ stoichiometry. Usually, the produced Heusler alloys are non-stoichiometric [7]. In addition, there are studies that analyzes the minority addition of a fourth element. It has been found that the addition of low amounts of Fe [8] or Co [9] causes a significant shift of transition temperatures. This displacement is favored by the modification of interatomic distances and hybridization. Consequently, it is a good option to design alloys with transitions in the desired temperature range for a particular application. For example, magnetic cooling near room temperature.

Nevertheless, there is a comparative lack of studies about cycling (heating–cooling). The correct functionality of MSM alloys largely depends on the stability of their response under the action of cyclic or repetitive processes. Most studies analyzing the cyclic process usually use only the first cycle. At most after a heat treatment of the sample to be analyzed. Among the studies that have analyzed behavior after multiple cycles are the following [12–14]. In Ni–Mn–Sn base alloys, an improvement in the cyclical

✉ A. Wederni
asma.wederni@ehu.eus

✉ J. J. Suñol
joanjosep.sunyol@udg.edu

[1] Department of Physics, Campus Montilivi S/N, University of Girona, 17003 Girona, Spain

[2] Department of Applied Physics, EUPDS, UPV/EHU, 20018 San Sebastian, Spain

[3] Department of Chemistry, College of Science, Qassim University, 51452 Buraidah, Saudi Arabia

Published online: 19 October 2023

stability of the mechanical response to compression and the elastocaloric effect has been noted [12]. The same effects have been found in Ni–Mn–In base alloys [13]. On the other hand, in Ni–Mn–Ga–Co–Cu Heusler microwires, high stability after cycling has also been noted, retaining a good mechanical response [14]. The calorimetric analysis, especially with differential scanning calorimetry (DSC), is needed to check the thermal stability after cycling. DSC has been widely used in MSM alloys to determine: a) transformation temperatures and b) thermodynamic parameters: enthalpy and entropy [10, 11].

In the present work, two Heusler-type Ni–Mn–Sn (with a minor addition of Pd) alloys have been subjected to hundred cycles of heat treatment, inducing the reversible structural transformation. The analysis of the thermal, structural and thermomagnetic studies have benn done to compare the results before and after the thermal cycling process.

Materials and methods

Concerning samples production, two alloys $Ni_{49}Mn_{36}Sn_{14}Pd_1$ and $Ni_{48}Mn_{36}Sn_{14}Pd_2$ have been synthesized with ribbon shape. The elements Ni, Mn, Sn, Pd (Sigma-Aldrich) have been used as precursors, with a purity ≥ 99.5%. The first step has been the production of the bulk alloys using the arc-melting technique (Bühler MAM-1). Casting is carried out in a controlled atmosphere, argon (with a vacuum prior to the introduction of argon of 10^{-4} torr). This process has been repeated four times in order to facilitate specimen homogenization. Then, the massive ones have been melted (in argon-controlled atmosphere, 400 mbar) using an induction system, and their rapid solidification has been carried out in a melt-spinning equipment (Bühler MSP 10), using a linear speed on the surface of the equipment wheel of 40 m/s and an injection pressure of 1000 mbar). The produced ribbons dimensions are around 1 mm wide and about 20 µm thick.

The crystalline structure at room temperature of the ribbons has been characterized by XRD performed at room temperature (Bruker, D500 S). The analysis of diffraction patterns has been carried out using the Rietveld's method and the MAUD software. The thermal characterization has been carried out by DSC (DSC822, Mettler-Toledo), in argon atmosphere and heating/cooling rate of 10 K/min. Thermal cycles have been carried out between room and liquid nitrogen temperatures, by introducing/extracting the samples in a reservoir of liquid nitrogen. In this processing, the alloys have been 30 s at each temperature. The magnetic and thermomagnetic analysis has been carried out by magnetic hysteresis cycles (at 50 and 300 K), and with zero-field cooling (ZFC), field cooling (FC) and field heating (FH) processes in a PPMS 6000 Quantum Design equipment, from low temperature to 400 K and applying magnetic fields of 50 Oe and 50 kOe.

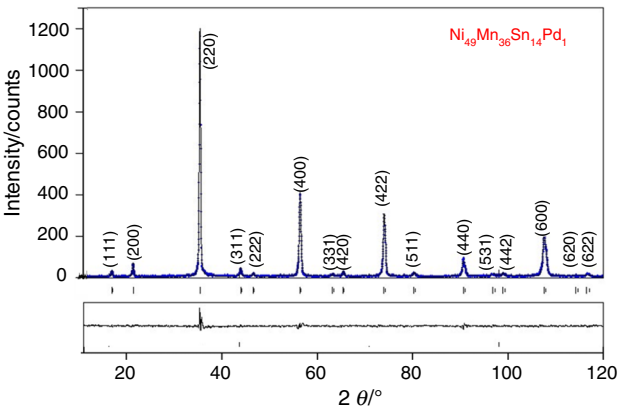

Fig. 1 XRD diffraction pattern (room temperature) and Rietveld refinement of the alloy $Ni_{49}Mn_{36}Sn_{14}Pd_1$

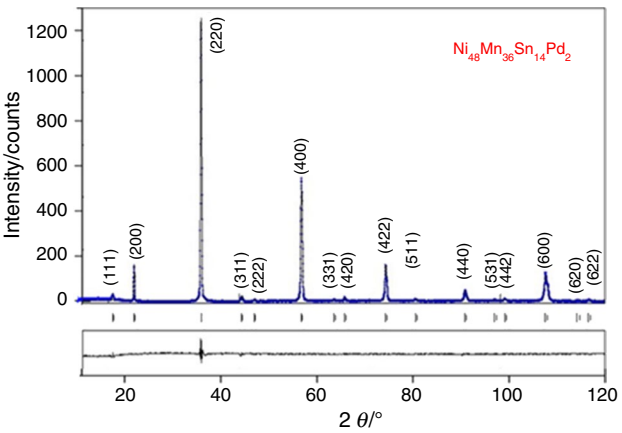

Fig. 2 XRD diffraction pattern (room temperature) and Rietveld refinement of the alloy $Ni_{48}Mn_{36}Sn_{14}Pd_2$

Results and discussion

Structural analysis

The characterization of the crystalline structure at room temperature of alloys produced and subjected to hundred thermal cycles allows us to state whether its structure corresponds to an austenite or to a martensite. Figures 1 and 2, respectively, show the diffractograms corresponding to the alloys $Ni_{49}Mn_{36}Sn_{14}Pd_1$ and $Ni_{48}Mn_{36}Sn_{14}Pd_2$. The structure obtained is austenitic, $L2_1$, which means that if there is a structural transformation, it is below room temperature. It should be noted that if none of the superstructure peaks typical of Heusler alloys were detected, indexed crystallographic

Table 1 Crystalline parameters obtained from Rietveld refinement and the $L2_1$ order parameter

Composition at.%	Lattice parameter /nm	Microstrain	Crystalline size /nm	$L2_1$ order /%
$Ni_{49}Mn_{36}Sn_{14}Pd_1$ (Before cycling)	0.5993(2) [17]	0.546(8)	101(3)	56
$Ni_{49}Mn_{36}Sn_{14}Pd_1$ (After cycling)	0.5989(3)	0.432(6)	108(2)	58
$Ni_{48}Mn_{36}Sn_{14}Pd_2$ (Before cycling)	0.6001(2) [17]	0.597(7)	109(3)	54
$Ni_{48}Mn_{36}Sn_{14}Pd_2$ (After cycling)	0.5994(2)	0.478(5)	118(2)	67

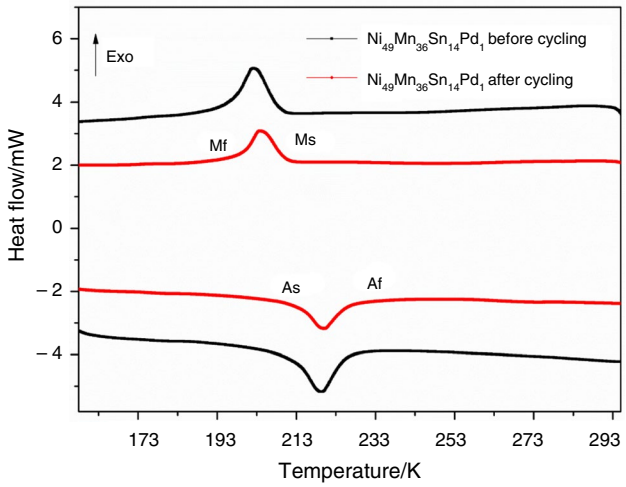

Fig. 3 DSC cooling/heating scan at 10 K/min of the alloy $Ni_{49}Mn_{36}Sn_{14}Pd_1$. Cooling up scans, heating down scans

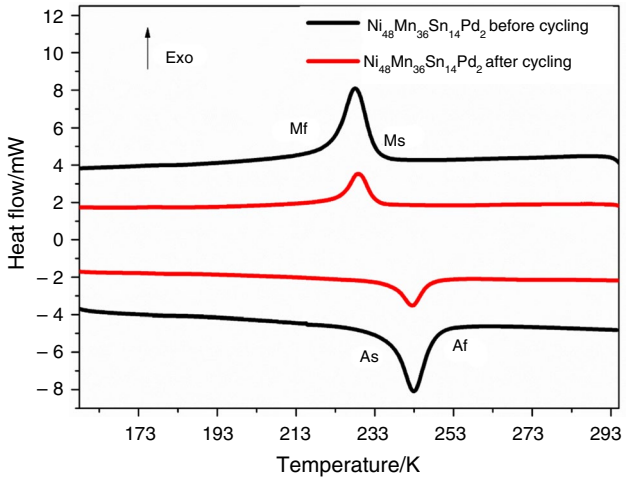

Fig. 4 DSC cooling/heating scan at 10 K/min of the alloy $Ni_{48}Mn_{36}Sn_{14}Pd_2$. Cooling up scans, heating down scans

peaks (h k l Miller indexes) such as 1 1 1, 3 1 1, 3 3 1, 5 1 1 or 5 3 1, the structure would be the cubic B2 with a lower degree of atomic order [15].

Table 1 shows the crystallographic parameters calculated using the Rietveld refinement method. There are parameters before and after cycling. Alloys (before 100 cycle) were previously partially analyzed [17]. Regarding XRD analysis, only lattice parameters were given in this referenced manuscript.

The cell parameter increases slightly by adding more Pd, expected effect as Pd is the atom with the largest atomic size. The addition of Pd in the crystallographic structure is in a substitutional form, not forming precipitates, a problem detected when Tb has been added in alloys of Ni-Mn-Sn [12]. Regarding the effect of cycles, there is a slight decrease in the lattice parameter and the microstrain index, together with an increase in crystal size. The continuous cycles favor small microstructural changes by decreasing the density of crystallographic defects (vacancies, dislocations) introduced during the mechanical process (decreasing the microstrain) (Figs. 3 and 4).

It is known that the degree of order is one of the parameters influencing the martensitic transformation temperature [17]. The alloys are far from the Heusler 2:1:1 stoichiometry. Thus, it is expected a $L2_1$ order degree (S_{111}) lower than 100%. The $L2_1$ order degree has been evaluated using the Webster model [18], expressed as:

$$S_{111} = \sqrt{\frac{I_{111,\mathrm{exp}}/I_{111,\mathrm{theo}}}{I_{220,\mathrm{exp}}/I_{222,\mathrm{theo}}}} \cdot 100$$

where with subscript '111/220' and 'exp/theo' is the XRD peak intensity of 111 or 2200 peaks in the experimentally XRD patterns or in the theoretical ones for the $L2_1$ phase. An increase in the order parameter is found, specially, in alloy with 2 at-% of palladium.

Thermal analysis

A small compositional change can cause a significant displacement of transformation temperatures. However, this displacement is usually associated with the e/a parameter, which corresponds to the average outer electrons [19]. In this case, since there are 10 that contribute both the Ni ($3d^8\ 4s^2$) and the Pd ($4d^{10}$), this effect is negligible.

The transition temperatures are given in Table 1, M_s and M_f are the martensite start and martensite finish temperatures

Table 2 Characteristic temperatures obtained from DSC heating/cooling scans

Composition at.%	M_s / K	M_f / K	A_s / K	A_f / K	T_o / K	T_{AM} / K	T_{MA} / K
$Ni_{49}Mn_{36}Sn_{14}Pd_1$ (Before cycling)	206.9	190.1	208.9	223.8	215.4	197.8	215.1
$Ni_{49}Mn_{36}Sn_{14}Pd_1$ (After cycling)	203.8	192.3	208.2	225.4	214.6	201.1	216.3
$Ni_{48}Mn_{36}Sn_{14}Pd_2$ (Before cycling)	230.9	216.8	232.2	246.7	238.8	225.8	241.2
$Ni_{48}Mn_{36}Sn_{14}Pd_2$ (After cycling)	232.3	218.9	233.8	247.2	239.8	227.1	240.3

Table 3 Thermodynamic parameters obtained or calculated from the analysis of the DSC heating/cooling scans

Composition at.%	Δ H /J g^{-1}	Δ S /J g^{-1} K^{-1}	Δ S_i /J g^{-1} K^{-1}	E_{el} /J g^{-1}	W_d /J g^{-1}
$Ni_{49}Mn_{36}Sn_{14}Pd_1$ (Before cycling)	1.44	0.00669	0.28	0.112	0.053
$Ni_{49}Mn_{36}Sn_{14}Pd_1$ (After cycling)	1.35	0.0063	0.23	0.073	0.0431
$Ni_{48}Mn_{36}Sn_{14}Pd_2$ (Before cycling)	2.99	0.0125	0.41	0.177	0.0895
$Ni_{48}Mn_{36}Sn_{14}Pd_2$ (After cycling)	2.86	0.0119	0.34	0.160	0.0799

(cooling scan) and A_s and A_f are the austenite start and austenite finish temperatures (heating scan). Values are higher in alloy with 2 at.% of palladium. These temperatures are only slightly shifted after cycling. The equilibrium Gibbs temperature, T_o, has been calculated, following the procedure described in ref. [20]. This characteristic temperature is Pd content dependent and only slight shift is found after cycling. Thus, it can be stated that the thermal stability is not highly affected by cycling. The temperature interval of the transformation is defined as the difference between the peak temperatures of the austenite to martensite transformation, T_{AM}, and the reverse martensite to austenite transformation, T_{MA}. The values are reduced about 2 K after cycling (Table 2).

It is known that the characteristic temperatures are cooling/heating rate dependent and sometimes an apparent activation energy was calculated [21]. Nevertheless, the general trend of the temperatures is expected to be similar. By analyzing the DSC scans, some thermodynamic parameters as the entropy and the entropy of the transformation have been calculated by integration [22]. The average values (cooling/heating) are shown in Table 3. Both enthalpy and entropy have been increased with the palladium addition. Cycling provokes a decrease around 10–12% of the values. Indicating that the heat release after cycling is lower. Probably, the accommodation of the martensitic phase and the reduction of microstructural defects favor this reduction.

The thermal and thermodynamic analysis has been applied to estimate other thermodynamic parameters as the irreversible entropy change, ΔS_i [23], the elastic energy, E_{el} [24] or the irreversible dissipated energy, W_d [25]. The procedure and equations involved are described in [23–26]. All these parameters are higher in alloy with 2 at.% Pd and decreases with cycling. It is the same tendency found in the enthalpy and the entropy of the structural transformation.

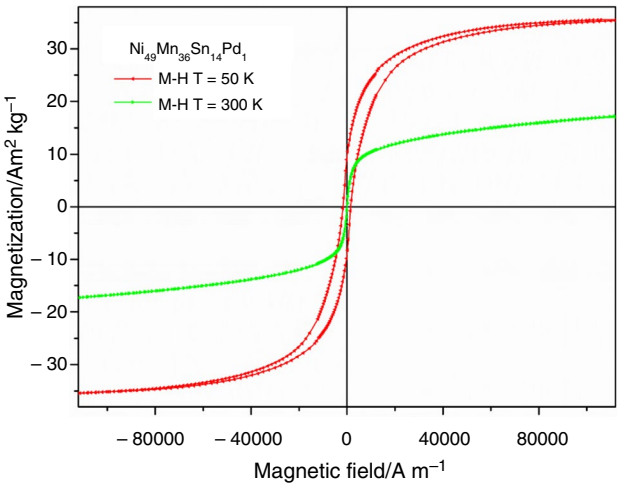

Fig. 5 Ferromagnetic hysteresis cycles at 50 and 300 K of the alloy $Ni_{49}Mn_{36}Sn_{14}Pd_1$

Thermomagnetic analysis

In addition to the stability of the crystalline structure and thermal stability, in magnetic alloys with shape memory, the stability of their magnetic and thermomagnetic response is decisive in reference to their applicability. Consequently, it is customary to complement thermal measurements with thermomagnetic measurements [11, 27].

The magnetic hysteresis cycles of the two alloys have been carried out, at 50 and 300 K. The curves obtained are shown in Figs. 5 and 6 for alloys $Ni_{49}Mn_{36}Sn_{14}Pd_1$ and $Ni_{48}Mn_{36}Sn_{14}Pd_2$, respectively. The differentiated behavior at both temperatures is due to the fact that at 300 K, the phase is austenite, while at 50 K the martensite. Though it should be taken into account that at 300 K, the sample is close to the paramagnetic state that also determines the

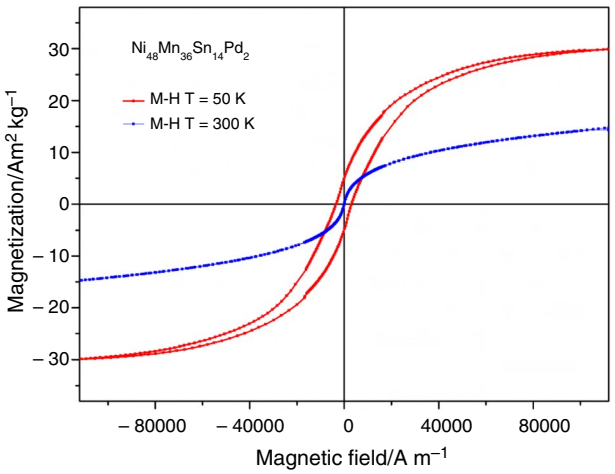

Fig. 6 Ferromagnetic hysteresis cycles at 50 and 300 K of the alloy $Ni_{48}Mn_{36}Sn_{14}Pd_2$

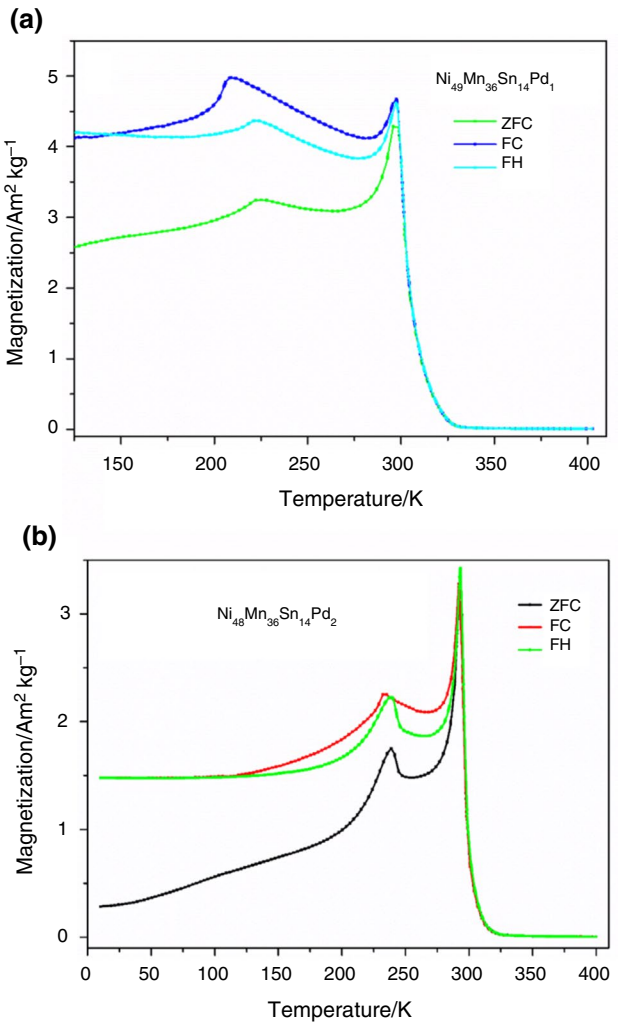

Fig. 7 Thermomagnetic ZFC–FC–FH scans (at 50 Oe) of the alloys $Ni_{49}Mn_{36}Sn_{14}Pd_1$ (up) and $Ni_{48}Mn_{36}Sn_{14}Pd_2$ (down)

hysteresis loop–low coercivity, M versus H dependence is approaching to linear. The increment of the palladium addition provokes an increase in the coercivity. The coercivity increased from 25 to 39 Oe at 300 K and from 243 Oe to Oe 351 at 50 K. This behavior is associated with the microstrain, higher the microstrain higher the coercivity of the alloy. The coercivity of samples not subjected to thermal cycles follows the same tendency. However, after cycling, the values decrease by around 10% (effect also due to the reduction in the density of crystallographic defects). The magnetization of saturation is near to be achieved and it is lower when measured at 300 K; as expected due to the high magnetization of the ferromagnetic martensite. The same tendencies been detected in Ni-Mn-Sn alloys doped with copper [28]. The main difference is that the magnetization of saturation lowers also about a 10% after cycling. Probably palladium atoms tend to occupy Ni atomic sites in the Heusler structure, affecting the total average magnetic moment.

Concerning the thermomagnetic measurements, the FH, FC and ZFC curves between 10 and 400 K have been measured following the procedure described in ref. [29]. Figures 7 and 8 show the magnetic scans performed at 50 Oe and 50 kOe, respectively. It is known that the FC and ZFC curves display information about the reversible and irreversible processes owing to the hysteresis cycle (heating/cooling) associated with the reversible structural transformation (austenite to martensite). The temperatures associated with the transformation are similar (at 50 Oe) to those detected in DSC scans. Slight shift is due to the application of the external magnetic field. For example, the temperatures of martensite start are 201.5 K and 221 K for alloys Ni49Mn-36Sn14Pd1 and Ni48Mn36Sn14Pd2. At high temperature, it has been detected the magnetization decay due to the ferromagnetic to paramagnetic transition.

Upon cooling, we observe a rapid growth from 200 to 250 K for the ZFC, FC and FH processes. This indicates the martensite's Curies transition (TCM) [16].

The characteristic Curie temperatures are close to 320 K in both alloys. The peaks near the Curie temperature are attributed to the Hopkinson effect [30]. As this temperature is higher to the structural transformation temperatures, it is the Curie temperature of the austenite phase. However, the separation of the ZFC and FC scans at temperatures below the structural transformation is provoked by the coexistence of antiferromagnetic and ferromagnetic states and/or a spin glass state [31]. At high field (5 T), the structural transformation is well defined while at low field (50 Oe) the separation between FC and FH curve is observed in higher temperature range from 100 to 300 K that could suggest existence of usability of the magnetic structure.

As expected, the increase in the external magnetic field provokes an increase in the magnetization of the samples.

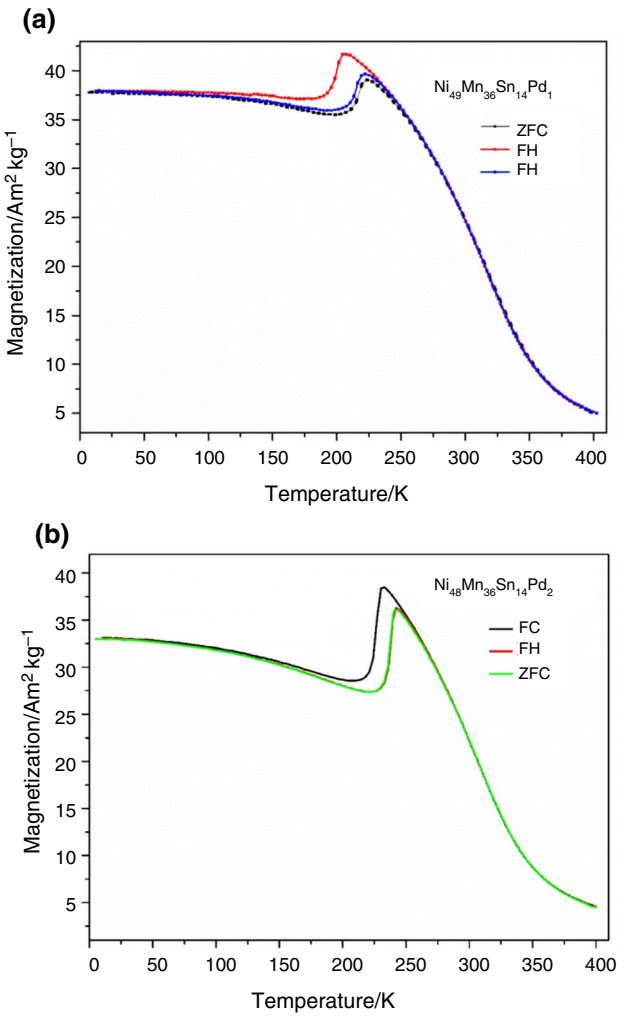

Fig. 8 Thermomagnetic ZFC–FC–FH scans (at 50 kOe) of the alloys $Ni_{49}Mn_{36}Sn_{14}Pd_1$ (up) and $Ni_{48}Mn_{36}Sn_{14}Pd_2$ (down)

These values are higher in the alloy with only 1 at.% of palladium, because of the reduction of nickel content. Furthermore, it is also fund a slight shift of the characteristic temperatures. The martensite start temperatures are (at 50 kOe) 199 K and 220 K for alloys $Ni_{49}Mn_{36}Sn_{14}Pd_1$ and $Ni_{48}Mn_{36}Sn_{14}Pd_2$. This effect can be associated with a kinetic arrest as previously found in Mn–Co–Sb specimens [32]. It was expected a higher stabilization of the martensite phase as increasing the applied magnetic field. Nevertheless, a high stability of the temperatures under different applied fields is a key factor for the specimen applicability.

Regarding the comparison with the samples before thermal cycling, the magnetization of saturation is reduced about 10%. Similar tendency to that detected in ferromagnetic hysteresis cycles. However, the structural transformation is shifted to low temperatures; at 50 Oe, the martensite start temperatures were 208.7 and 233.3 K (before cycling) for alloys $Ni_{49}Mn_{36}Sn_{14}Pd_1$ and $Ni_{48}Mn_{36}Sn_{14}Pd_2$ [16]. Thus, it is found an increase in the stability of the austenite phase, probably due to the reduction of crystallographic defects in the parent $L2_1$ phase. Likewise, it has been detected a slight increase in the Curie temperature (310 K before cycling, 320 K after cycling). It indicates a thermal stabilization of the ferromagnetic phase, probably due to the best ordered magnetic moments due to the atomic positions in the samples after reducing the density of crystallographic defects.

Conclusions

The thermal and thermomagnetic stability after cycling of two nanocrystalline alloys have been checked. Two nanocrystalline alloys have been produced, of compositions $Ni_{49}Mn_{36}Sn_{14}Pd_1$ and $Ni_{48}Mn_{36}Sn_{14}Pd_2$ (at.%). These ferromagnetic alloys have been subjected to a hundred of thermal cycles around the reversible and hysteretic martensitic transformation.

Concerning the XRD microstructural analysis, the crystallographic structure at room temperature is the cubic austenite Heusler $L2_1$. It has been found that cycles favor a decrease in the density of crystallographic defects in both alloys. The microstrain index is reduced from 0.546 to 0.432 and from 0.597 to 0.478. Also, an increase in the order parameter $L2_1$, from 0.56 to 0.58% and from 54 to 67%. Thus, cyclic processes favor structural ordering.

Thermodynamic parameters (entropy and enthalpy) show a decrease of around 10–12%. Thus, the heat involved in the structural transition after cycling has been reduced, probably by minimizing the heat release provoked by the crystallographic defects and a non-optimal atomic order. Likewise, higher enthalpy and entropy have been found by increasing palladium content.

Regarding the thermomagnetic response, it is reduced by about 12%. Thus, cyclic processes favor magnetic ordering. It also provokes a slight increase, about 10 K, in the Curie temperature, stabilizing the ferromagnetic phase. Effect probably due to an optimized average magnetic moment due to the best ordered atoms in the $L2_1$ austenite structure.

Acknowledgements The authors would like to thank the financial support of Spanish Mineco project MAT2016-75967-P and University of Girona PONT2020-01 project.

Author contributions AW contributed to formal analysis and investigation. MI contributed to formal analysis. MK contributed to supervision. JJS contributed to writing—original draft and conceptualization.

Funding Open Access funding provided thanks to the CRUE-CSIC agreement with Springer Nature.

References

1. Yu GH, Xu YL, Liu ZH, Qiu HM, Zhu ZY, Huang XP, Pan LQ. Recent progress in Heusler type magnetic shape memory alloys. Rare Met. 2015;34:527–39. https://doi.org/10.1007/s12598-015-0534-1.
2. Tavares S, Yang KS, Meyers MA. Heusler: past, properties, new alloys, and products. Progress Mater Sci. 2023;132:101017. https://doi.org/10.1016/j.pmatsci.2022.101017.
3. Coll R, Escoda L, Saurina J, Sánchez-Llamazares JL, Hernando B, Suñol JJ. Martensitic transformation in Mn-Ni-Sn Heusler alloy. J Thermal Anal Calorim. 2010;99:905–9. https://doi.org/10.1007/s10973-009-0489-2.
4. Zheng D, Jing C, Lu B, Li Z, Xu K. Martensitic transformation, magnetocaloric effect and phase transition strain in $Ni_{50}Mn_{36-x}Ge_xSn_{14}$ Heusler alloy. Rare Met. 2016;41:4217–22. https://doi.org/10.1007/s12598-016-0820-6.
5. Huang XM, Zhao Y, Yan HL, Tang S, Yang YQ, Jia N, Yang B, Li ZB, Zhang YD, Esling C, Xiang Z, Liang Z. A first-principle assisted framework for designing high elastocloric Ni-Mn- based magnetic shape memory alloy. J Mater Sci Technol. 2023;134:151–62. https://doi.org/10.1016/j.jmst.2022.06.041.
6. Wei ZY, Shen Y, Zhang Z, Guo JP, Li B, Ek Liu, Zhang ZD, Liu J. Low-pressure-induced giant barocaloric effect in all-d-metal Heusler $Ni_{35.5}Co_{14.5}Mn_{35}Ti_{15}$ magnetic shape memory alloy. APL Mater. 2020;8:051101. https://doi.org/10.1063/5.0005021.
7. Yan HL, Huang XM, Esling C. Recent progress in crystallographic characterization, magneto responsive and elastocaloric effects of Ni–Mn–In based Heusler alloys—a review. Front Mater. 2022;9: 812984. https://doi.org/10.3389/fmats.2022.812984.
8. Chen CT, Yu L, Zhu JC, Tan CL. The mechanical properties of Ni–Mn–Sn alloy thin films with Fe doping. Integr Ferroelectr. 2020;207:156–65. https://doi.org/10.1080/10584587.2020.1728675.
9. Xia QH, Tan CL, Han BL, Tian XH, Zhao L, Zhao WB, Ma TY, Wang C, Zhang K. Strain engineering in Ni–Co–Mn–Sn magnetic shape memory alloys: Influence on the magnetic properties and martensitic transformation. Materials. 2022;15:5889. https://doi.org/10.3390/ma15175889.
10. Vidal-Crespo A, Manchón-Gordón AF, Blazquez JS, Ipus JJ, Svec P, Conde CF. Thermal arrest analysis of the reverse martensitic transformation in a $Ni_{55}Fe_{19}Ga_{26}$ alloy obtained by melt-spinning. J Thermal Anal Calorim. 2023;148:2367–75. https://doi.org/10.1007/s10973-022-11889-1.
11. Aydogdu Y, Turabi AS, Aydogdu A, Kok M, Yakinci ZD, Karaca HE. The effects of boron addition on the magnetic and mechanical properties of NiMnSn shape memory alloys. J Thermal Anal Calorim. 2016;126:399–406. https://doi.org/10.1007/s10973-016-5576-6.
12. Gui W, Qu Y, Cao Y, Zhao Y, Liu C, Zhou Q, Chen J, Liu Y. The effect of Tb substitution for Ni on microstructure, martensitic transformation and cyclic stability of elastocaloric effect in Ni–Mn–Sn shape memory alloys. J Mater Res Tech. 2022;19:4998–5007. https://doi.org/10.1016/j.jmrt.2022.07.018.
13. Yang Z, Cong DY, Sun XM, Nie ZH, Wang YD. Enhanced cyclability of elastocaloric effect in boron-microalloyed Ni–Mn–In magnetic shape memory alloys. Acta Mater. 2017;127:33–42. https://doi.org/10.1016/j.actamat.2017.01.025.
14. Zhang J, Ding Z, Hou R, Gao J, Zhu J. Giant high temperature superelasticity in $Ni_{53}Mn_{24}Ga_{21}Co_1Cu_1$ microwires. Intermetallics. 2020;122: 106799. https://doi.org/10.1016/j.intermet.2020.106799.
15. Xu X, Nagasako M, Ito W, Umetsu RY, Kanomata T, Kainuma R. Magnetic properties and phase diagram of $Ni_{50}Mn_{50-x}Ga_x$ ferromagnetic shape memory alloys. Acta Mater. 2013;61:6712–23. https://doi.org/10.1016/j.actamat.2013.07.033.
16. Wederni A, Ipatov M, Pineda E, Escoda L, González JM, Khitouni M, Suñol JJ. Martensitic transformation, thermal analysis and magnetocaloric properties of Ni–Mn–Sn–Pd alloys. Processes. 2020;8:1582. https://doi.org/10.3390/pr8121582.
17. Liu J, Scheerbaum N, Hinz D, Gutfleish O. Martensitic transformation and magnetic properties in Ni–Fe–Ga–Co magnetic shape memory alloy. Acta Mater. 2008;56:3177–86. https://doi.org/10.1016/j.actamat.2008.03.008.
18. Li Z, Hayashi K, Dong J, Li JF, Miyazaki Y. Distinct impact of order degree on thermoelectric power factor of p-type full-Heusler Mn_2VAl compounds. Mater Res Express. 2020;7: 055503. https://doi.org/10.1088/2053-1591/ab875b.
19. Zarinejad M, Wada K, Pahlevani F, Katal R, Rimaz S. Valence electron ratio for design shape memory alloys with desired phase transformation temperatures. Shap Mem Elasticity. 2021;7:179–89. https://doi.org/10.1007/s40830-021-00319-0.
20. Kaufman L, Hullert M. Thermodynamics of martensite transformation. In: Olson GB, Owen WS, editors. Martensite. Cambridge: ASM International; 1992. p. 41–8.
21. Bachagha T, Rekik H, Krifa M, Suñol JJ, Khitouni M. Investigation of the enthalpy/entropy variation and structure of Ni-Mn-Sn (Co, In) melt spun ribbons. J Thermal Anal Calorim. 2016;126:1463–8. https://doi.org/10.1007/s10973-016-5716-z.
22. Kok M, Yakinci ZD, Aydogdu A, Aydogdu Y. Thermal and magnetic properties of $Ni_{51}Mn_{28.5}Ga_{19.5}B$ magnetic-shape-memory alloy. J Thermal Anal Calorim. 2014;115:555–9. https://doi.org/10.1007/s10973-013-3365-z.
23. Coll R, Saurina J, Escoda L, Suñol JJ. Thermal analysis of $Mn_{50}Ni_{50-x}(Sn, In)_x$ Heusler shape memory alloys. J Thermal Anal Calorim. 2018;134:1277–84. https://doi.org/10.1007/s10973-018-7551-x.
24. Qader IN, Ercan E, Faraj BAM, Kok M, Dagdelen F, Aydogdu Y. The influence of time-dependent aging process on the thermodynamic parameters and microstructures of quaternary Cu79-Al12-Mi4-Nb5 (wt.%) shape memory alloy. Iran J Sci Technol A. 2020;44:903–10. https://doi.org/10.1007/s40995-020-00876-6.
25. Shamberger PJ, Ohuchi FS. Hysteresis of the martensite phase transition in magnetocaloric effect of Ni-Mn_Sn alloys. Phys Rev B. 2009;79: 144407. https://doi.org/10.1103/PhysRevB.79.144407.
26. Dagdelen F, Ozay C, Ercan E, Emir G, Qader IN. Change of electrical resistivity during phase transitions in NiMnSn-based shape memory alloy. J Thermal Anal Calorim. 2022;147:5815–23. https://doi.org/10.1007/s10973-021-10927-8.
27. Aydodgu Y, Turabi AS, Boddeti B, Saghaan SE, Aydogdu A, Kilik G, Abboosh O, Karaca HE. Shape memory behavior of $Ni45Mn40Co5Sb_{10-x}B_x$ magnetic shape memory alloys. J Thermal Anal Calorim. 2016;143:127–37. https://doi.org/10.1007/s10973-019-09172-x.

28. Wederni A, Ipatov M, González JM, Khitouni M, Suñol JJ. Ni-Mn-Sn-Cu alloys after thermal cycling: thermal and magnetic response. Materials. 2021;14:6851. https://doi.org/10.3390/ma14226851.
29. Wederni A, Ipatov M, Pineda L, Suñol JJ, Escoda L, González JM, Alleg S, Khitouni M, Zuberek R, Chumak O, Nabialek A, Lynnyk A. Magnetic properties, martensitic and magneto-structural transformations of ferromagnetic Ni-Mn-Sn-Cu shape memory alloys. Appl Phys A. 2020;126:320. https://doi.org/10.1007/s00339-020-03489-3.
30. Hopkinson, J. Magnetic and other physical properties of iron at a high temperature. Philos Trans R Soc London A. 1889, 443–465.
31. Wang H, Zhang H, Tan YW, Huo D. Spin glass feature and exchange bias effect in Pt/antiferromagnetic $LaMnO_3$ heterostructure. J Phys Cond Matter. 2021;33: 285802. https://doi.org/10.1088/1361-648X/ac0023.
32. Tekgil A, Acet M, Farle, Unal N. Kinetic arrest of the ferrimagnetic state in indium-doped Mn182Co018Sb. J Alloys Comp. 2017;695:418–25. https://doi.org/10.1016/j.jallcom.2016.11.093.